Analysis Proposal

Benedikt Riedel

January 21, 2014

1 Detector Stability

Analysis of the detector stability using of partial detectors, 40-string though 79-string configuration, in [1] and [2] showed that there was significant noise due to the freeze-in process. For the full detector, the same effect is seen, see Figure 1 and 2. After solid ice is formed, the annular modulation of the atmospheric muon rate with atmospheric temperature, see Figure 3, causes the detector rate to have a sinusoid-like time dependence. This becomes the most significant contribution to detector instability over time. Similar affects can be seen in the detector SLC rate, see Figure 4.

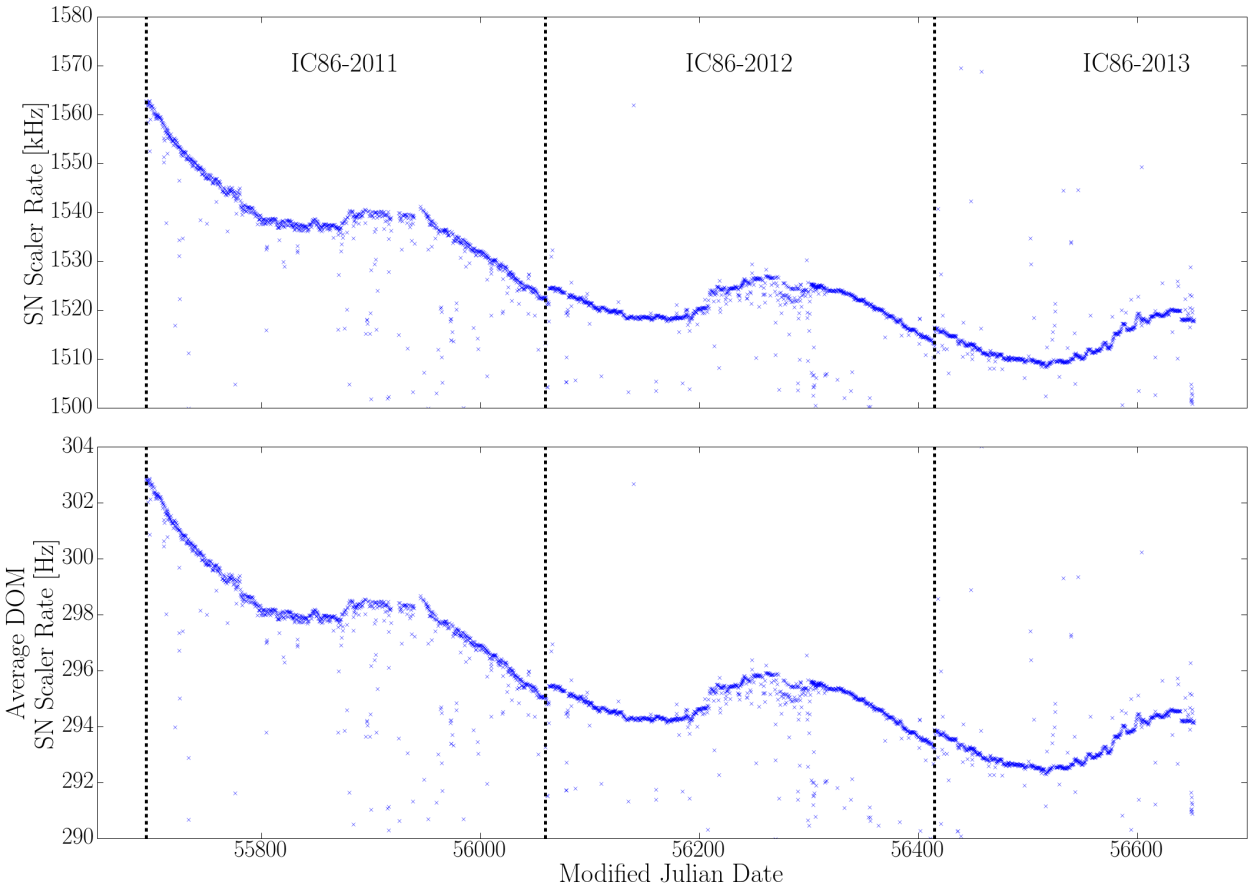

Figure 1: Total (Top) and Average (Bottom) Supernova Scaler Rate as function of time. The seasonal variation of the muon rate can be seen as a sinusoid-like pattern in the data, while the affect of the freeze-in can be seen clearly in the rate decay in IC86-2011. There is also a continual decay in rate of unknown origin. Note: Top plot is in Kilohertz, while bottom plot is in Hertz.

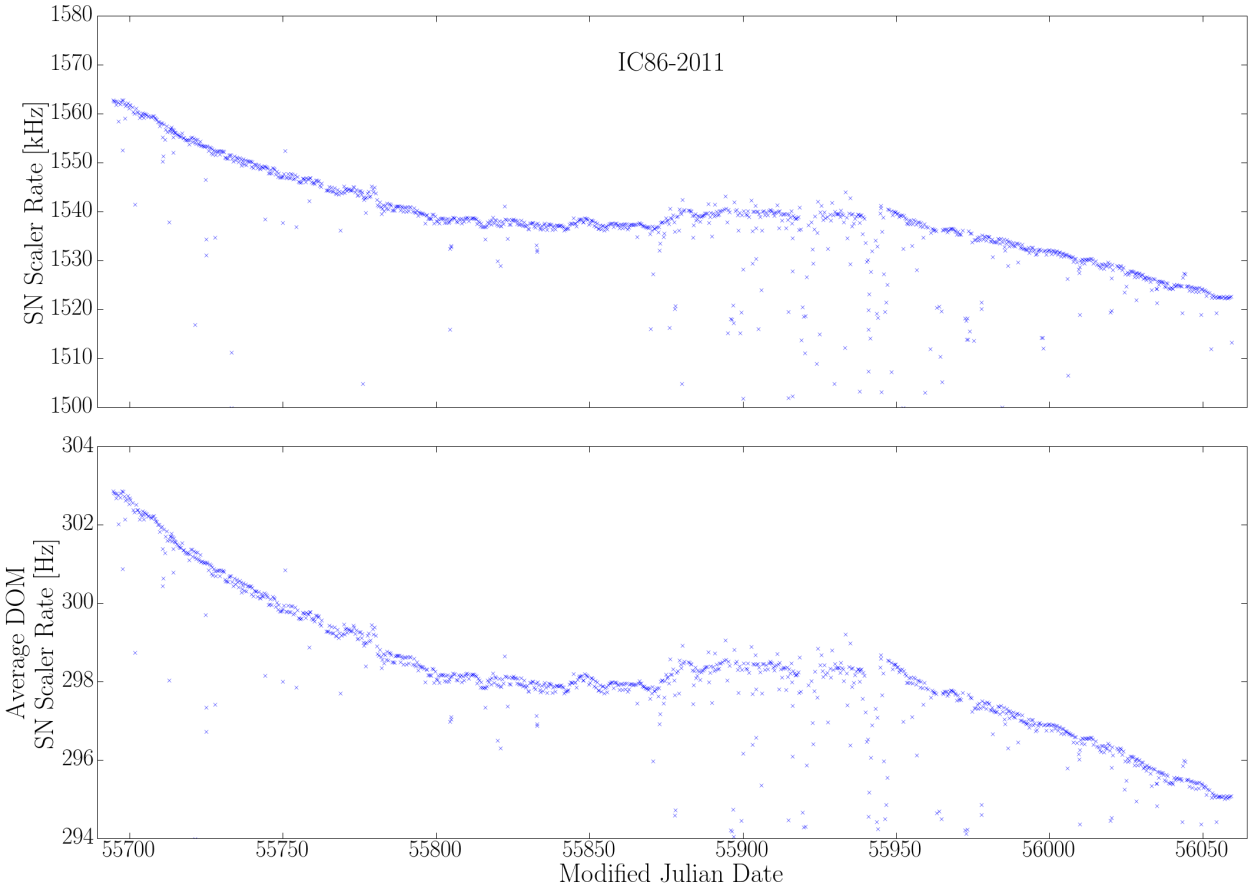

Figure 2: Total (Top) and Average (Bottom) Supernova Scaler Rate as function of time for the first year of IC86, IC86-2011. The freeze-in process dominates the rate over the course of the first half of IC86-2011, but becomes subdominant due to effects from muons.
Note: Top plot is in Kilohertz, while bottom plot is in Hertz.

Figure 1 and 4 also reveal a continual decay in the detector rate throughout the operation of the full detector configuration. Comparison of supernova scaler rate for the 86-string configuration for strings deployed at different construction cycles, see Figure 5, shows that the decay is on-going even several years after deployment. Similarly, the freeze-in progresses has a depth dependence, see Figure 6 and [2]. The origin of this decay is unknown. There are multiple possible explanations that can be examined from the data:

- Construction effects: Continuation of the freeze-in process
- Detector effects: Detector aging and drift of detector settings away from optimal values

The freeze-in process continues even after the ice appears to be solid, as shown by the "Swedish Camera", a camera system deployed in the deep ice at the end of String 80. Recordings from the "Swedish Camera" have shown that the ice surrounding the bore hole continues to change over the years. The air and particles trapped in the ice from drilling and refilling the bore holes are being pressed into a central column. This processes appears to be on-going and may cause low levels of triboluminescence similar to those associated with the solidification process that are seen as a decay in the supernova scaler.

To establish the decay rate for the individual DOMs, a fit of:

$$R(t) = A + R_{\mu}(t) + (C\exp(-\tau t)) \tag{1}$$

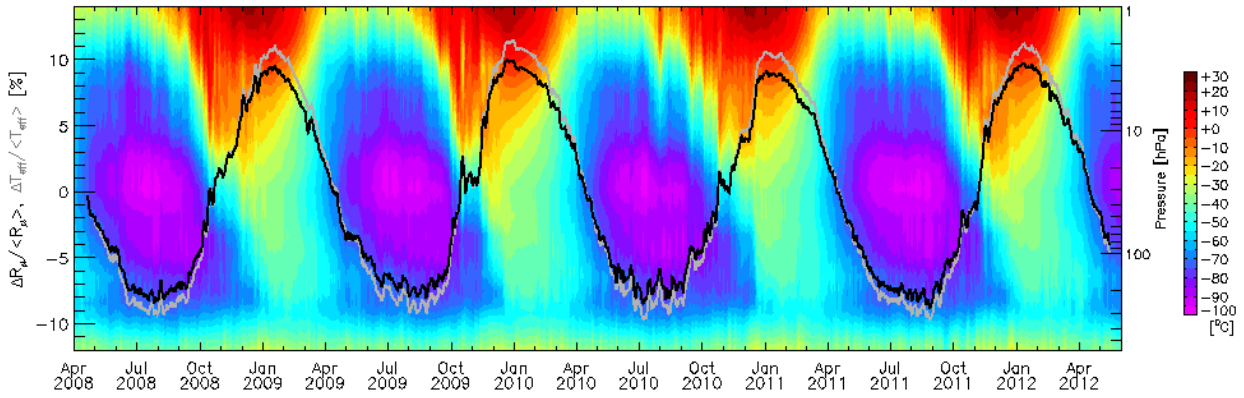

Figure 3: Black line shows muon rate seasonal modulation as percentage deviation from average. For reference, the atmospheric temperature as a percentage deviation from average in grey and atmospheric pressure.

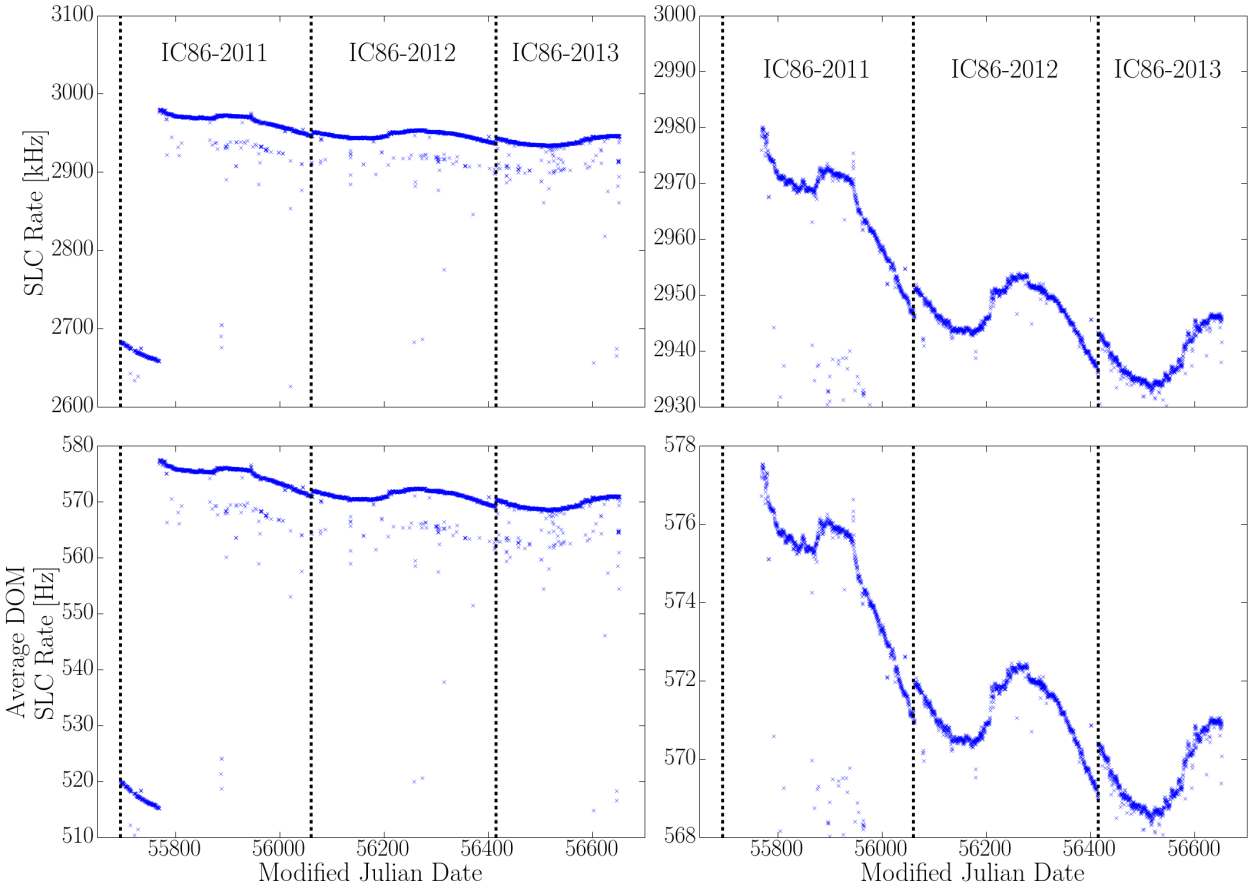

Figure 4: Total (Top Panels) and Average (Bottom Panels) SLC as function of time. The seasonal variation of the muon rate can be seen as a sinusoid-like pattern in the data, while the affect of the freeze-in can be seen in the decay in the rate over the course IC86-2011 to -2013. The jump in rate about a quarter into IC86-2011 is due to changes in the deadtime by a factor of 10 (0.25% to 0.025%) and the subsequent addition of non-Poissonic noise to the SLC rate.
Note: Top plots are in Kilohertz, while bottom plots are in Hertz.

where A is baseline noise from the DOM, R_μ is the time-dependent atmospheric muon rate contribution to the scaler rate, and $C\exp(-\tau t)$ is the contribution of the decay rate to the SN scaler rate, has to be performed on the SN scaler rate. [1] used the IceCube trigger-level data to estimate the atmospheric muon contribution. This data however has a significantly higher energy threshold, $\approx 400 - 800\,\text{GeV}$ depending on depth versus $\approx 1\,\text{TeV}$ and lower rate than the scaler data, i.e. $\approx 2100\,\text{Hz}$ versus $\approx 5200\,\text{Hz}$.

The HLC rate for individual DOMs from the pDAQ log-files provides an estimate of the atmospheric muon effect with a lower energy threshold. This HLC rate mimics the effect of the atmospheric muons, see Figure 7. A correction factor, R_C, has to be subtracted from the HLC rate, as there are HLCs due to noise. Assuming that the SLC rate is purely Poissonic, R_C can be estimated using

$$R_C = 2\Delta t R_3 \left(R_1 + R_2 + R_4 + R_5\right) \tag{2}$$

where R_3 is the rate of the central DOM, and $R_{1,2,4,5}$ is the rate of the surrounding DOMs. The rate for each DOM is estimated using the SLC rate for each DOM. The remaining rate can be attributed to the effect of atmospheric muons, see Figure **??**.

The response to atmospheric muons is different for SN scaler rate and the HLC rate. SN scalers have a much longer deadtime compared to SLC and HLC rates, $250\,\mu$s versus $\approx 2.5\,\mu$s. The HLC rate requires two DOMs to participate, while SN scalers is sensitive to individual DOMs. This is predominately a concern for DOMs on the edge of the detector. The definition of A and $R_\mu(t)$ from Equation 1 has to therefore be changed slightly to estimate the atmospheric muon contribution to the SN scaler rate. A absorbs the average atmospheric muon rate that effect the SN scalers, while $R_\mu(t)$ becomes the deviation of the atmospheric muon rate from this average. Equation 1 is more aptly described by

$$R(t) = R + R_\mu + B\Delta R_{\text{HLC}}(t) + (C\exp(-\tau t)) \tag{3}$$

where

$$\Delta R_{\text{HLC}}(t) = R_{\text{HLC}}(t) - \langle R_{\text{HLC}} \rangle \tag{4}$$

and B is scaling factor that compensates for the difference in HLC and SN scaler sensitivity. B can be found by letting it freely float while fitting for τ in Equation 3. This subtraction method has already proven usable to reduce the affect of atmospheric muons ont the SLC rate, see Figure 9. If the fitting does not work properly one can estimate the scaling factor by simulating atmospheric muons without detector noise and determine if the scaling factor of SLC atmospheric muons rate to HLC atmospheric muons rate as a function of energy.

Effects from detector aging would be hard to disentangle from difference in the DOM components between different revisions of the DOM hardware and possible freeze-in effects. Further long-term studies with the DOMs in the freezer at Physical Science Laboratory would be necessary.

A drift of detector settings away from optimal values should be detectable from changes in the time constant of supernova scaler decay rate between strings deployed at the different construction cycles and during physics run transitions, respectively. A drift away from optimal values should be detectable by a jump or sink in the supernova scaler during the run transition. A jump in the detector rate was found during the physics run transitions, see Figure 1. This jump can be attributed to the addition of previously removed DOMs from the detector configuration, see bottom plot of Figure 1, and to slight shifts in the detector settings.

2 Muon Background

Over the course of the last several years the frequency and supernova significance, ξ, of false supernova alerts has risen, see Figure 10. [1] showed that atmospheric muons are main cause of false triggers and are correlated to the muon hit rate, see Figure **??**. The nature of these muons beyond the number of DOMs they trigger however was not explored. The rising significance of the alerts was initially attributed to increasing solar activity as the sun approached the maximum of the 11-year solar cycle, see Figure 11, as the temperature of the upper atmosphere rises with increasing solar irradiation. The rise in the significances should not be significantly effected by these long-term effects to the flux or energy spectrum of the atmospheric muons, as

the background region is defined over significantly shorter timespan than these effects. The question remains whether there are distinct features in these events that can be extracted from the information provided by the DAQ.

In [1] the Data Storage and Transmission (DST) data was used determine the muon hit rate from the SMT8 trigger rate and the number of DOMs that were triggered, "nchannel" (nchan), of the triggers. This muon hit rate is shown to be correlated to ξ as determined by the the SNDAQ online analysis. There was however no consideration for other triggers, such as the *String Trigger* and the *Volume Trigger*. These triggers could help identify large muon events that cause false supernova triggers more readily as they are sensitive to the geometry of the event rather than just the total number of DOMs hit. For this reason, a study of the correlation of trigger rates for SMT8, SMT3, Volume Trigger, and String Trigger with supernova false trigger will be performed. For the supernova false triggers with $\xi > 6$, the trigger rate for all triggers of interest will be determined from the Super Data Storage Tape (sDST). The sDST data contains all individual triggers and time stamps thereof. The DST data only contains a bitmask that accounts for the the presence of a trigger, but not a count. This will help in account for possible overlapping triggers and give a better picture of the timing distribution. In order to ensure proper comparison of the data, the same rolling window as used in the SNDAQ online analysis is applied to the sDST data. The data is than split into the background and signal region and comparison of the trigger rates, nchannel distributions, and direction of events will be performed.

Investigating other triggers will remove some of the shortcomings of the analysis in [1]:

- SMT8 rate of DST data does not reflect the real SMT8 rate
- SMT8 trigger does not consider any geometry information beyond the local coincidence (LC) condition
- Supernova scalers have a lower energy cutoff than SMT8, i.e. is SMT8 the best possible measure or is there a different trigger?

The DST does not contain all the trigger information, as overlapping triggers are compressed into a bitmask that only accounts for the the presence of a trigger, but not a count. SMT8 triggers can overlap because of their extended readout windows as required by the EventBuilder. The probability of overlap of two SMT8, assuming 2100 Hz trigger rate for SMT8 and a 10 μs readout overlap window, is $\approx 0.2\%$. This should have an minuscule effect on the correlation method. When looking at all possible triggers the overlap between different triggers approaches 1. Additional other triggers, mainly the *Volume Trigger*, have a much higher rate (≈ 3300 Hz), which leads to a much higher possibility of overlap for these triggers.

The SMT8 trigger does not consider the geometry of the events and the detector beyond the geometry requirement of the local coincidence (LC) condition. The geometry and time span of a muon event are completely different than that for a supernova event. Individual muon events would only illuminate certain areas of the detector for $\mathcal{O}(1 - 10\,\mu\text{s})$, while the supernova event illuminates the entirety of the detector over the course of $\mathcal{O}(1 - 10\,\text{s})$. Looking at triggers that do have stricter geometric constrains may help identifying muon events. Also the *Volume Trigger*'s much higher rate may yield more information about lower energy muons that the supernova scalers are sensitive to, but not SMT8.

In addition to the trigger rate aspect. The comparison of nchan distribution and the location of the "center-of-gravity", where most of the hits are clustered, of the events between the signal region and the background region will be performed.

3 Ice Efficiency

The optical properties of the ice in which IceCube is embedded are not uniform throughout the detector. One of the main assumptions that goes into the supernova onlien analysis is that of a uniform illumination of the ice by the interaction of supernova neutrinos. The different optical properties however will cause the ice to not be illuminated uniformly, as some DOMs will have greater sensitivity than others because the light from the products of supernova neutrino interactions can travel more readily through the ice.

From studying the ice properties versus depth for MeV-scale positrons, one can establish an efficiency factor for the ice surrounding the DOM. To do this, an average of the effective volume of the DOMs outside the dust layer is calculated for an IceCube. The DOMs in the dust layer are excluded from the average

because of the poor optical properties of the ice. This causes an articifical decrease of the average effectice volume. The ratio between the average and the effective volume for the DOM is defined as the ice efficiency parameter.

$$\epsilon_{\text{Ice}} = \frac{V_{\text{eff}}}{\langle V_{\text{eff}} \rangle} \tag{5}$$

The effective volume of the DeepCore DOMs has to adjusted from the higher quantum efficiency as this effect is already taken into account separately, but still be able to compensate for their different location inside the detector. To observe the effect on the online analysis, the online analysis is performed again on the IC86 data set.

References

[1] V. Baum, Verbesserung Der Supernova-Detektion Mit Dem IceCube-Neutrinoteleskop, Johannes Gutenberg-Universität Mainz, 2011.

[2] M. Krasberg, Low-Level Commissioning, IceCube Collaboration Meeting Baton Rouge, 2006

[3] D. Hathaway and M. Adams, Solar Cycle Prediction, `http://solarscience.msfc.nasa.gov/predict.shtml`, NASA Marshall Space Flight Center, 2014

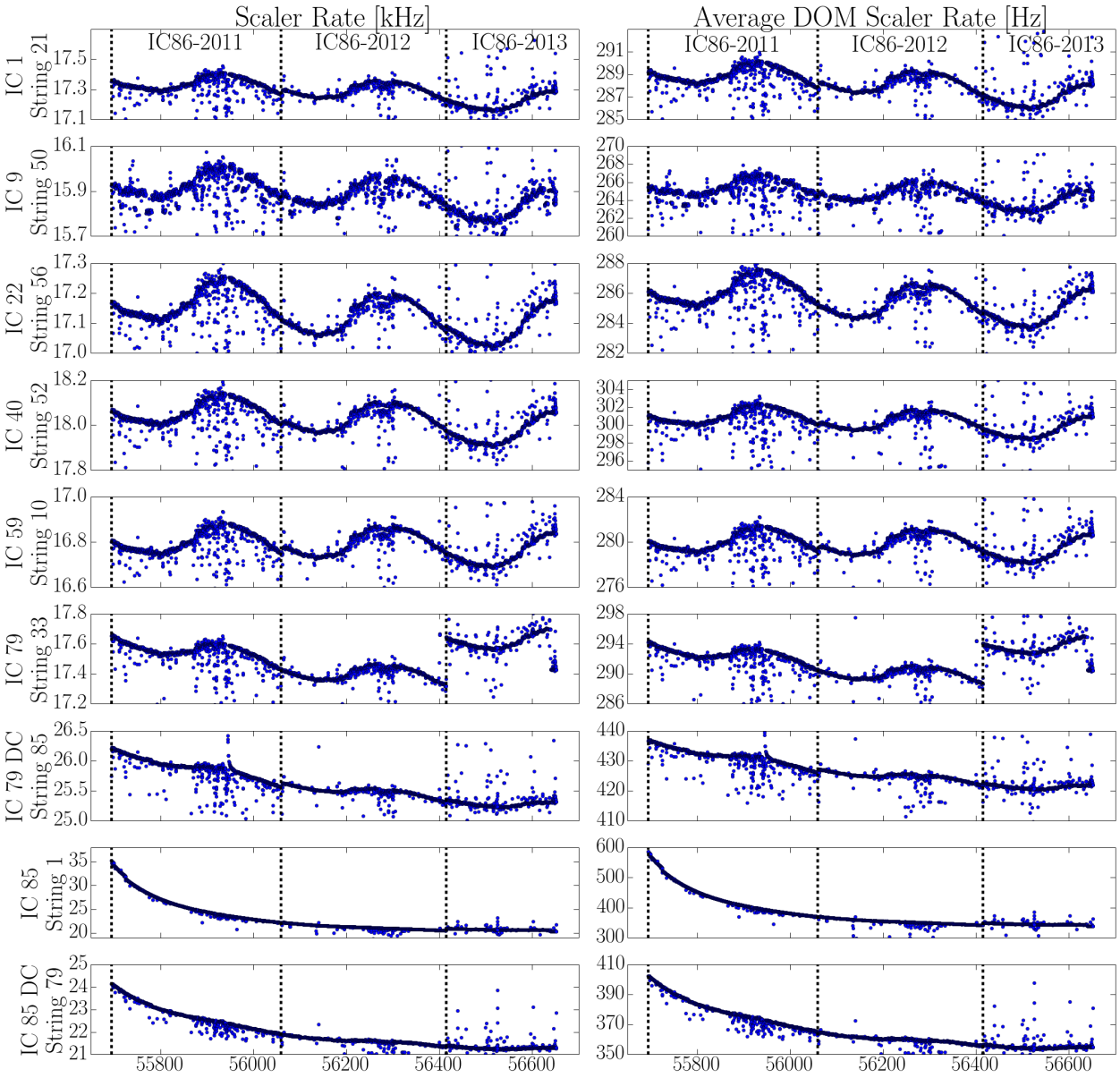

Figure 5: Supernova Scaler Rate of Strings that have been deployed at different generations of the detector. String 21 for IC1, String 50 for IC9, String 56 for IC22, String 52 for IC40, String 10 for IC59, String 33 for IC79, String 85 for IC79 DeepCore, String 1 for IC86, String 79 for IC85 DeepCore.

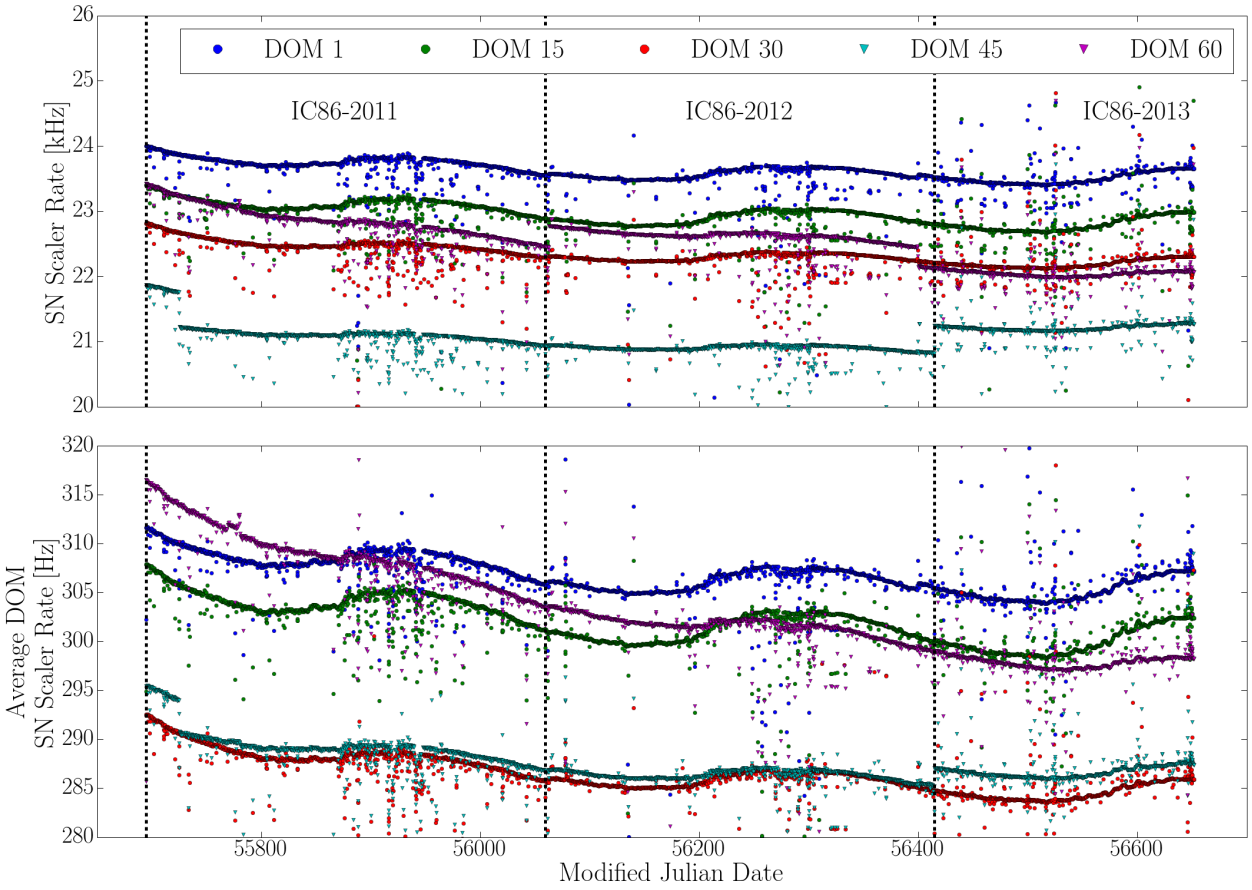

Figure 6: Supernova Scaler Rate of DOMs at different depths. DOM 1 are DOMs at the top of the detector, DOM 15 are in the middle of the top half, DOM 30 are in middle and inside the dust layer, DOM 45 are in the middle of the bottom half of the detector, and DOM 60 are the bottom of the detector. This excludes the DOMs from DeepCore as their geometry is different.

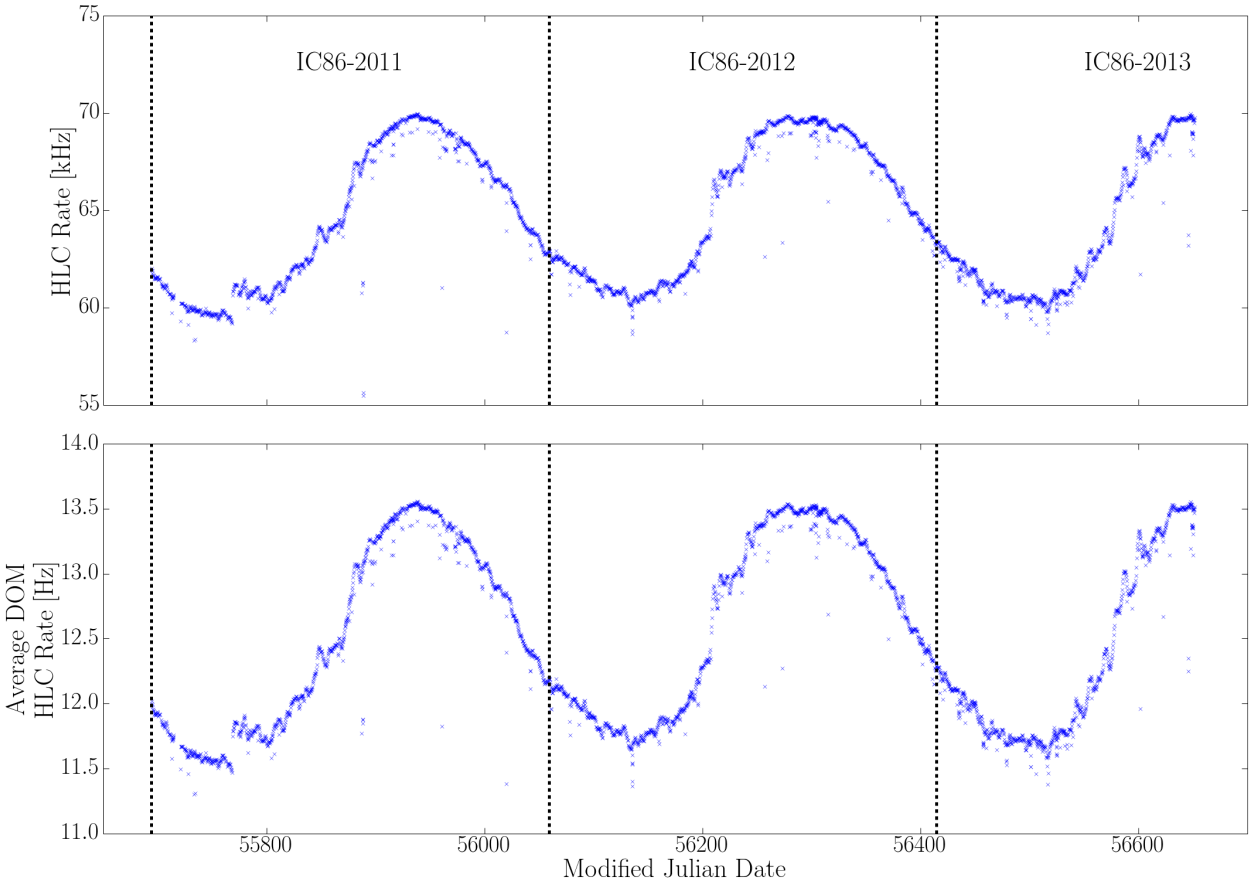

Figure 7: Total (Top) and Average (Bottom) HLC as function of time.

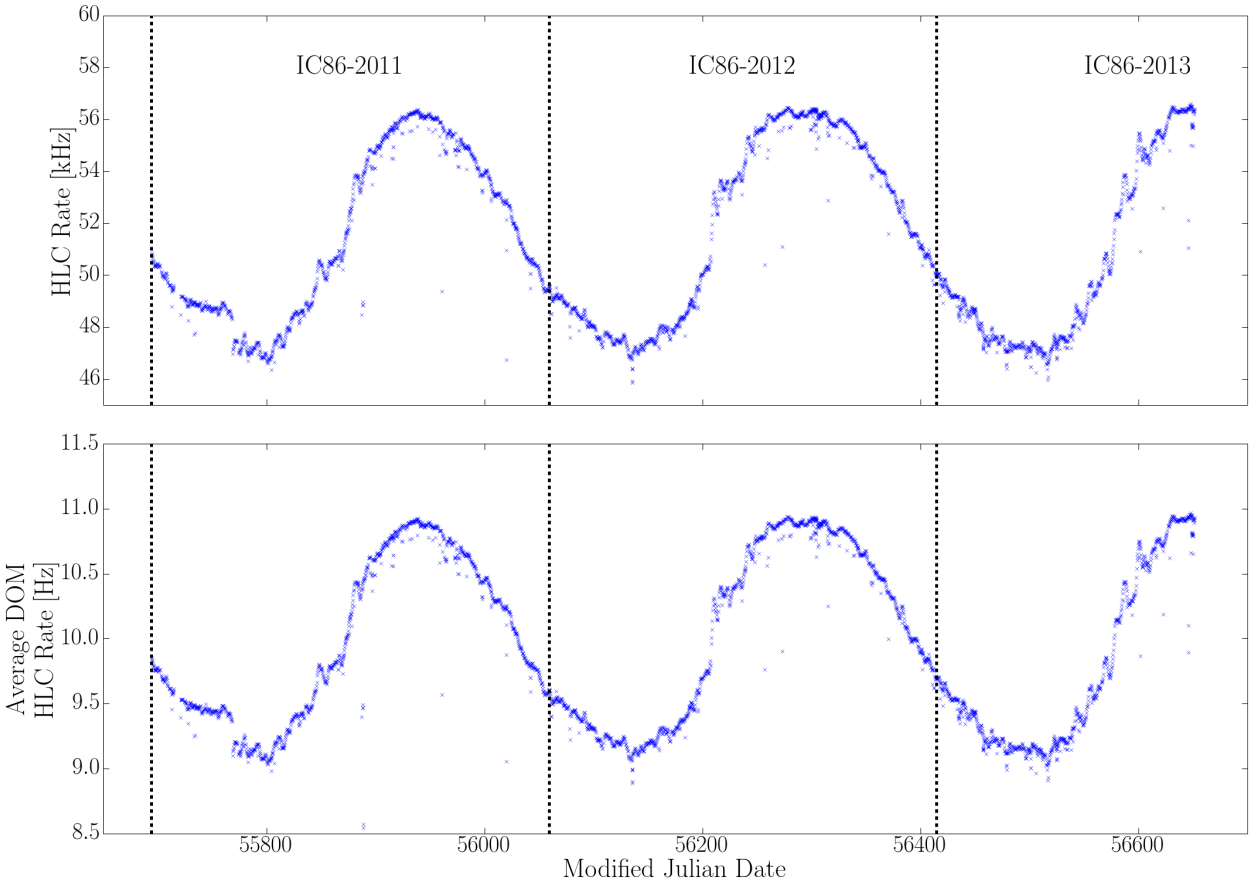

Figure 8: Total (Top) and Average (Bottom) HLC as function of time after coincidence rate is removed.

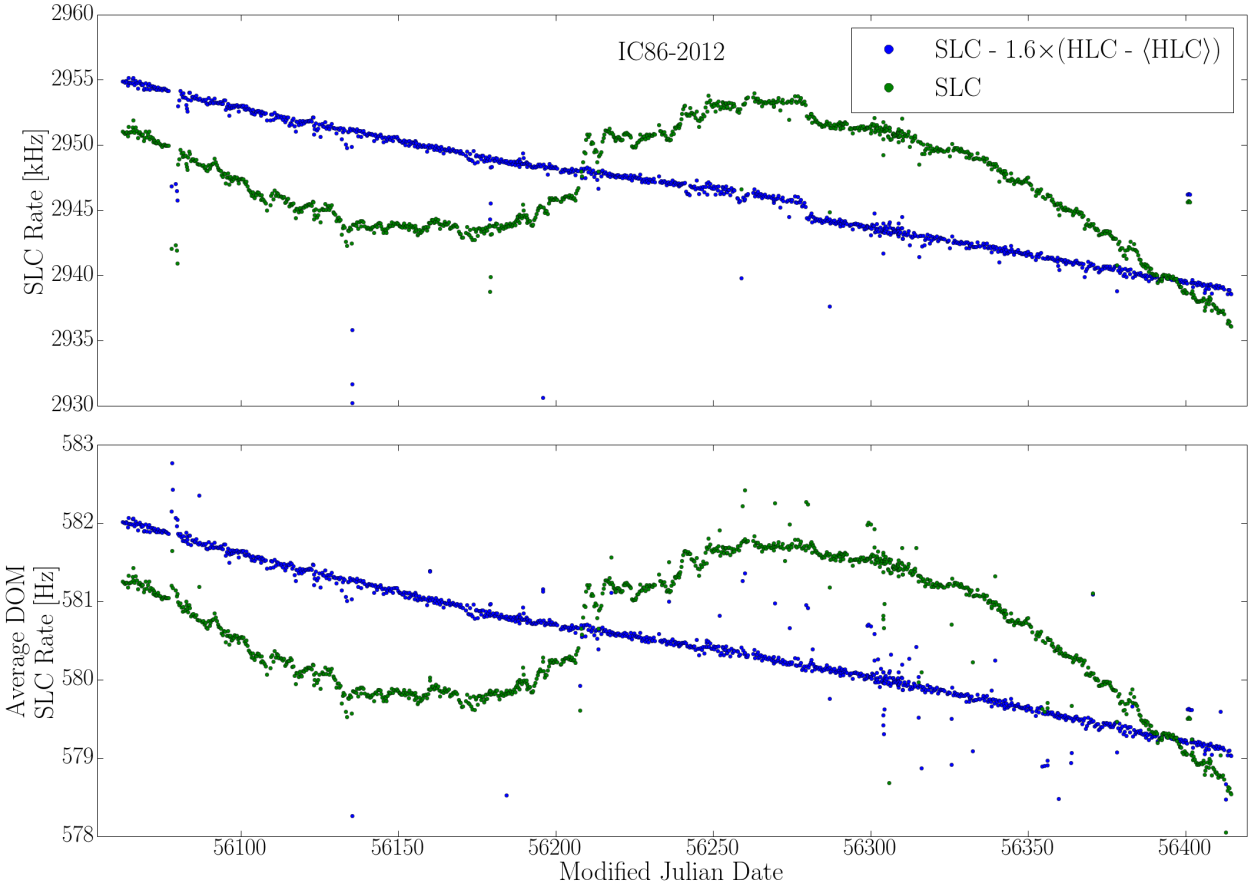

Figure 9: Total (Top) and Average (Bottom) SLC as function of time for IC86-2012 with and without muon substraction

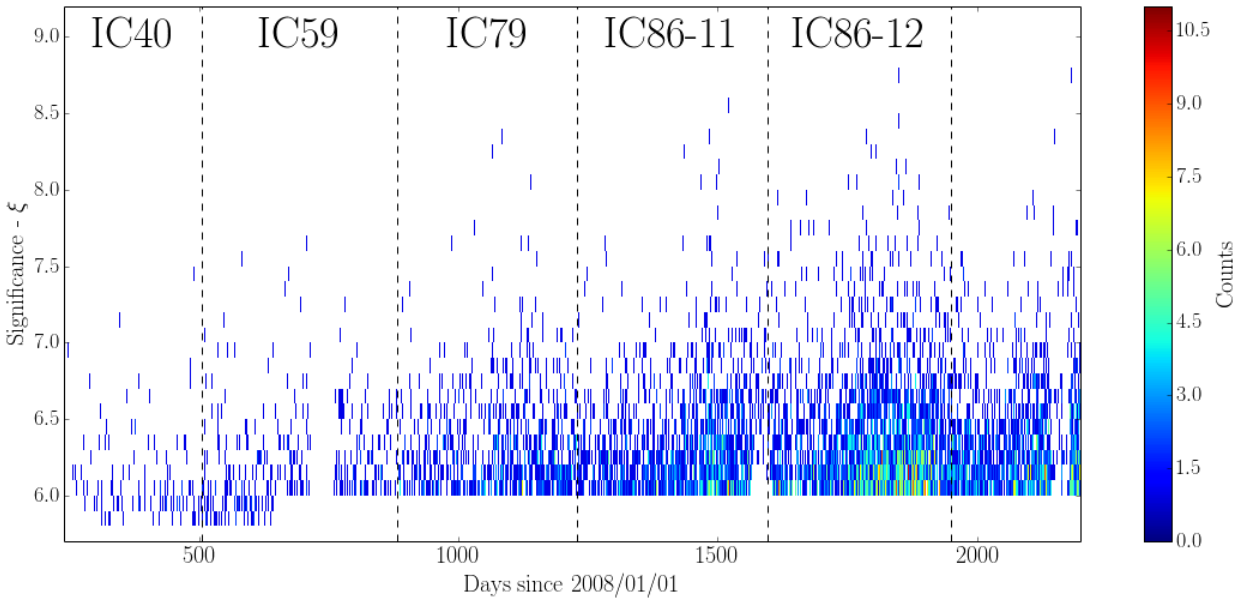

Figure 10: SNDAQ significances, ξ, over threshold (6) from IC40 to present.

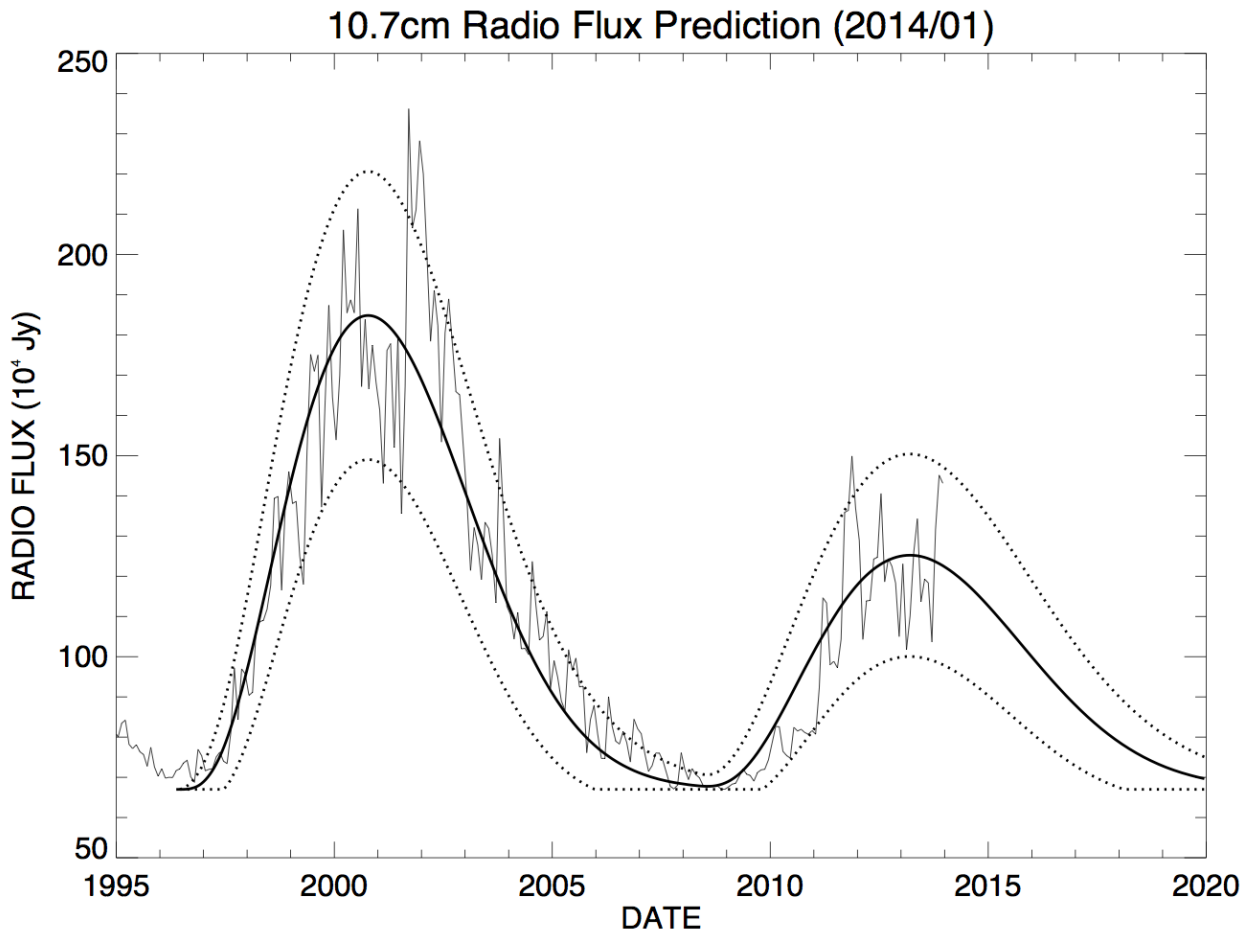

Figure 11: 10.7 cm (2.8 GHz) Radio Emission from the Sun as a function of time. This emission is a good tracer for UV emission that effects atmospheric density and thereby of atmospheric muon flux. The dashed lines prediction at 5% and 95%. The solid like is a prediction at 50%. [3]